Article

Deposition Precipitation for the Preparation of Carbon Nanofiber Supported Nickel Catalysts

Martijn K. van der Lee, Jos van Dillen, Johannes H. Bitter, and Krijn P. de Jong

J. Am. Chem. Soc., **2005**, 127 (39), 13573-13582• DOI: 10.1021/ja053038q • Publication Date (Web): 09 September 2005

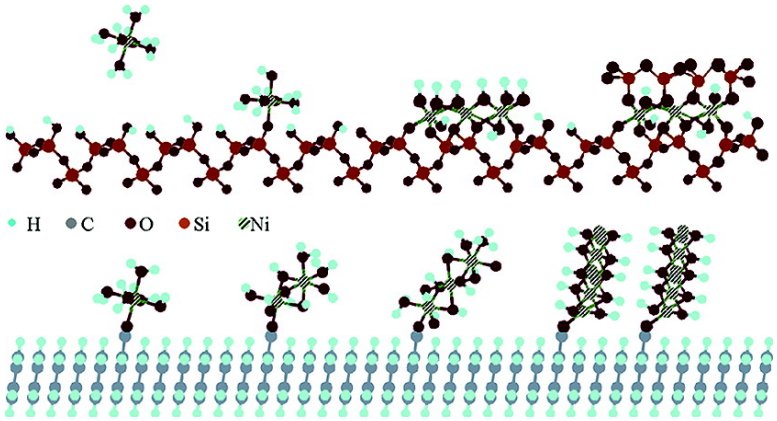

More About This Article

Additional resources and features associated with this article are available within the HTML version:

- Supporting Information
- Links to the 15 articles that cite this article, as of the time of this article download
- Access to high resolution figures
- Links to articles and content related to this article
- Copyright permission to reproduce figures and/or text from this article

View the Full Text HTML

J|A|C|S
ARTICLES
Published on Web 09/09/2005

Deposition Precipitation for the Preparation of Carbon Nanofiber Supported Nickel Catalysts

Martijn K. van der Lee, A. Jos van Dillen, Johannes H. Bitter, and Krijn P. de Jong*

Contribution from the Department of Inorganic Chemistry and Catalysis, Debye Institute, Utrecht University, P.O. Box 80 083, 3508 TB Utrecht, The Netherlands

Received May 10, 2005; E-mail: k.p.dejong@chem.uu.nl

Abstract: Deposition precipitation of nickel hydroxide onto modified carbon nanofibers has been studied and compared to deposition onto silica. The carbon nanofiber support materials consisted of graphite-like material of the fishbone-type with a diameter of 20−50 nm and a specific surface area of 150 m^2/g. Modification involved surface oxidation (CNF-O) optionally followed by partial reduction (CNF-OR) or thermal treatment (CNF-OT). Titration of the support materials showed the presence of 0.17 and 0.03 mmol/g carboxylic acid groups for CNF-O and CNF-OR, respectively. For the CNF-OT only basic groups were present. The deposition precipitation of 20 wt % nickel onto these supports has been studied by time dependent pH and nickel loading studies. With silica, nickel ion adsorption did not occur prior to nucleation of the nickel hydroxide phase at pH = 5.6. With CNF-O, nickel ion adsorption took place right from the start of the deposition process at pH = 3.5, and at pH = 5.6 already 4 wt % nickel was adsorbed. Nucleation of nickel hydroxide onto adsorbed nickel ion clusters proceeded subsequently. Characterization of the dried Ni/CNF-O samples with TEM and XRD showed well dispersed and thin (5 nm) platelets of nickel hydroxide adhering to the carbon nanofibers. After reduction at 773 K in hydrogen the Ni/CNF-O contained metallic nickel particles of 8 nm homogeneously distributed over the fibers. With CNF-OR and CNF-OT, precipitation of large platelets (> 500 nm) separate from the support took place. Clearly, the presence of carboxylic acid groups is essential to successfully deposit nickel hydroxide onto modified carbon nanofibers.

Introduction

Supported metal and metal oxide catalysts are indispensable for energy and chemical industries to reduce consumption of raw materials and to minimize the production of waste. Control over the preparation of supported metal catalysts is necessary to improve their key properties as activity, selectivity, and stability. The most important methodologies to prepare supported catalysts in both industry and academia involve impregnation and drying,[1−4] metal-ion adsorption,[5−8] deposition precipitation[9,10] and chemical vapor deposition.[11−12] Reviews on catalyst preparation are available from both a practical[13,14] and a fundamental point of view.[3,15]

The advent of nanostructured support materials such as ordered mesoporous materials,[16] carbon nanofibers,[17−20] and carbon nanotubes[21,22] provides opportunities for novel supported metal and metal oxide catalysts. Carbon nanofibers and carbon nanotubes are promising support materials in view of, among others, the control of surface properties, chemical inertness, the high accessibility, thermal stability, mechanical strength, and tunable bulk density. The field of carbon nanofiber supports has been pioneered by the groups of Baker,[23,24] Geus,[25] Ledoux,[26] and De Jong.[27,28] Recently, Serp and co-workers[29]

(1) Clause, O.; Kermarec, M.; Bonneviot, L.; Villain, F.; Che, M. *J. Am. Chem. Soc.* **1992**, *114*, 4709−4717.
(2) Van Dillen, A. J.; Terorde, R. J. A. M.; Lensveld, D. J.; Geus, J. W.; De Jong, K. P. *J. Catal.* **2003**, *216*, 257−264.
(3) Lekhal, A.; Glasser, B. J.; Khinast, J. G. *Chem. Eng. Sci.* **2004**, *59*, 1063−1077.
(4) Bergwerff, J. A.; Visser, T.; Leliveld, B. R. G.; Rossenaar, B. D.; De Jong, K. P.; Weckhuysen, B. M. *J. Am. Chem. Soc.* **2004**, *126*, 14548−14556.
(5) Regalbuto, J. R.; Navada, A.; Shadid, S.; Bricker, M. L.; Chen, Q. *J. Catal.* **1999**, *184*, 335−348.
(6) Schreier M.; Regalbuto, J. R. *J. Catal.* **2004**, *225*, 190−202.
(7) Carrier, X.; Lambert, J. F.; Che, M. *J. Am. Chem. Soc.* **1997**, *119*, 10137−10146.
(8) Negrier, F.; Marceau, E.; Che, M. *Chem. Commun.* **2002**, *11*, 1194−1195.
(9) Hermans, L. A. M.; Geus, J. W. *Stud. Surf. Sci. Catal.* **1979**, *3*, 113−130.
(10) Che, M.; Cheng, Z. X.; Louis, C. *J. Am. Chem. Soc.* **1995**, *117*, 2008−2018.
(11) Serp, P.; Kalck, P.; Feurer, R. *Chem. Rev.* **2002**, *102*, 3085−3128.
(12) Lashdaf, M.; Lahtinen, J.; Lindblad, M.; Venaelaeinen, T.; Krause, A. O. I. *Appl. Catal., A* **2004**, *276*, 129−137.
(13) Perego, C.; Villa, P. L. *Catal. Today* **1997**, *34*, 281−305.
(14) Campanati, M.; Fornasari, G.; Vaccart, A. *Catal. Today*, **2003**, *77*, 299−314.
(15) De Jong, K. P. *Curr. Opin. Solid State Mater. Sci.* **1999**, *4*, 55−62.
(16) Beck, J. S.; Vartuli, J. C.; Roth, W. J.; Leonowicz, M. E.; Kresge, C. T.; Schmitt, K. D.; Chu, C. T.-W.; Olson, D. H.; Sheppard, E. W.; McCullen, S. B.; Higgins, J. B.; Schlenker, J. J. L. *J. Am. Chem. Soc.* **1992**, *114*, 10834.
(17) Figueiredo, J. L.; Pereira, M. F. R.; Freitas, M. M. A.; Órfão, J. J. M. *Carbon* **1999**, *37*, 1379−1389.
(18) Rodríguez-Reinoso, F. *Carbon* **1998**, *36*, 159−175.
(19) De Jong, K. P.; Geus, J. W. *Catal. Rev.—Sci. Eng.* **2000**, *42*, 481−510.
(20) Helveg, S.; Lopez-Cartes, C.; Sehested, J.; Hansen, P. L.; Clausen, B. S.; Rostrup-Nielsen, J. R.; Abild-Pedersen, F.; Norskov, J. K. *Nature* **2004**, *427*, 426−429.
(21) Planeix, J. M.; Coustel, N.; Coq, B.; Brotons, V.; Kumbhar, P. S.; Dutartre, R.; Geneste, P.; Bernier, P.; Ajayan, P. M. *J. Am. Chem. Soc.* **1994**, *116*, 7935−7936.
(22) Iijima, S. *Nature* **1991**, *354*, 564.
(23) Baker, R. T. K.; Laubernds, K.; Wootsch, A.; Paal, Z. *J. Catal.* **2000**, *193*, 165−167.
(24) Salman, F.; Park, C.; Baker, R. T. K. *Catal. Today* **1999**, *53*, 385−394.
(25) Hoogenraad, M. S.; van Leeuwarden, R. A. G. M. M.; Van Breda Vriesman, G. J. B.; Broersma, A.; Van Dillen, A. J.; Geus, J. W. *Stud. Surf. Sci. Catal.* **1995**, *91*, 263−271.
(26) Vieira, R.; Pham-Huu, C.; Keller, N.; Ledoux, M. J. *Chem. Commun.* **2002**, *9*, 954−955.
(27) Toebes, M. L.; Prinsloo, F. F.; Bitter, J. H.; Van Dillen, J. A.; De Jong, K. P. *J. Catal.* **2003**, *214*, 78−87.

have written a review on the status of the use of carbon nanofibers (CNF) and carbon nanotubes (CNT) as support material. In this paper we will focus on the use of carbon nanofibers as support material while using deposition precipitation (DP) for the preparation of supported nickel catalysts. Nickel-based catalysts are widely used in processes such as hydrogenations, steam reforming, amination, and hydrodesulfurization.

Deposition precipitation involves the precipitation of a metal precursor onto a suspended support material. Usually precipitation is brought about by a controlled increase of the pH of an aqueous solution of the metal salt in question. Hydrolysis of urea typically at 363 K is a convenient method to slowly increase the pH. This method has been explored by Geus, Hermans, and Van Dillen[9,30] and De Jong,[31] and mechanistic studies have been published for nickel-on-silica by Burattin et al.[32−34] From these studies it is clear that nucleation and growth of the nickel compound, either turbostratic nickel hydroxide or nickel phyllosilicate, coincides with a significant interaction with the silica support. This interaction was studied by pH measurements during synthesis and by characterization of the loaded silica support materials.[9,31−35]

Deposition precipitation has hardly been studied for carbon-supported catalysts. Using activated carbon Wigmans[36] obtained nonuniform distributions of nickel over the support probably due to intraparticle diffusion limitation during precipitation. Prinsloo[37] prepared Fe/CNT and Co/CNT materials with low metal dispersion most likely due to a low interaction of the metal precursors with the carbon nanotubes. These results might be anticipated since the nature of the carbon support materials strongly deviates from the silica supports and the formation of mixed compounds of the metal precursor and the support is not possible.

Recently, we reported the preparation of highly loaded, well-dispersed nickel catalysts using DP with surface-oxidized CNF support material.[38] The mechanism of interaction during preparation was not discussed in this preliminary paper. Therefore, we have carried out a detailed study for the preparation of nickel-on-CNF catalysts using deposition precipitation and different types of surface-modified carbon nanofibers with surface groups ranging from acidic to basic. Titrations were done to assess the nature and the number of surface groups on the modified CNF. The measurement of pH during DP in combination with the extent of nickel removal from solution was used to obtain key information on nucleation and growth. These measurements were compared to experiments with a silica support under identical conditions of temperature and concentrations. The precipitated Ni/CNF catalysts were characterized both after drying and after reduction using in particular TEM and XRD.

Experimental Section

CNF Growth. Carbon nanofibers have been grown following the procedure described by Toebes et al.[39] Briefly, 1 g of calcined 20 wt % Ni/SiO_2 (particle size 425−850 μm) was placed in a quartz reactor and reduced with H_2 at 973 K. Subsequently, the catalyst was exposed to a flow of 400 mL/min that consisted of 20% H_2, 7% CO in N_2 at atmospheric pressure for 6 h. After the reactor was cooled, the product (∼5 g) was collected and coded as CNF-A. From the product silica was removed via a treatment in refluxing 1 M KOH solution for 2 h. The remaining product was refluxed in a mixture of concentrated nitric acid and sulfuric acid (1:1) for 30 min. This results in removal of the accessible nickel originating from the growth catalyst and surface oxidation of the carbon nanofibers. After being thoroughly washed, the carbon nanofibers were dried overnight at 393 K in air (code CNF-O).

To reduce the oxygen content of the carbon nanofibers, 0.5 g of CNF-O was thermally treated in a nitrogen flow of 100 mL/min at 873 K (heating rate 5 K/min) for 30 min. The thus obtained fibers were designated CNF-OT.

Another 0.5 g of CNF-O fibers was partly reduced with lithium aluminum hydride ($LiAlH_4$) under a dry nitrogen atmosphere. To this end 500 mg of CNF-O were suspended in 50 mL of freshly distilled THF, while 85 mg of $LiAlH_4$ (Merck) were suspended in 25 mL freshly distillated THF. Under nitrogen flow the $LiAlH_4$ suspension was carefully added to the CNF-O suspension and the total volume was subsequently stirred for 20 h. After reaction, the mixture was neutralized by slowly adding water to the suspension and resulting CNF were thoroughly washed with 1 M HCl and subsequently water. Finally the CNF were dried at 393 K for 18 h (CNF-OR).

CNF Acid−Base Titrations. Following previous literature[40] acid−base titrations were carried out using a titralab-TIM880 automatic titration setup equipped with a combined pH electrode and automatic burets. All titrations were carried out at room temperature using 50 mg of ground CNF support and 70 mL of water. During the titration N_2 gas was flushed over the liquid to avoid CO_2 to dissolve into the water. The titrations of the CNF supports were done after the addition of 5 mL of 0.10 M oxalic acid to the support slurry. After stabilization of the pH, titration with NaOH (0.010 M) was started and continued to pH 10. Also a blank experiment was done with 70 mL of H_2O and 5 mL of oxalic acid solution. The number of acid sites present on the CNF supports was determined by the difference in volume added compared to the blank. For example the difference in volume added between blank and sample at pH 8 provided the required amount of base to neutralize all groups with a $pK_a < 8$. For basic materials (CNF-OT) we report pK_b values rather than pK_a.

Nickel Deposition on CNF Materials. 20 wt % Ni on powdered CNF-O, CNF-OT, or CNF-OR were batchwise prepared via DP using aqueous solutions. A closed 350 mL reactor vessel equipped with baffels, pH electrode, thermometer, and magnetic stirrer was loaded with 250 mL of water, 300 mg of CNF support, and 371 mg of nickel nitrate hexahydrate (Acros 99%). The pH was adjusted to ∼3.5 by adding a few drops of diluted HNO_3 (Merck). After heating this mixture to 363 K, a solution of 230 mg of urea (Acros) in 3 mL of water was added. After 18 h, the slurry was cooled to room temperature and filtered. The loaded CNF were thoroughly washed and dried at 393 K for 18 h. The obtained supported nickel precursor was reduced in a 100 mL/min flow of 20 vol % hydrogen in nitrogen at 573 K (heating

(28) Toebes, M. L.; Zhang, Y.; Hajek, J.; Nijhuis, T. A.; Bitter, J. H.; Van Dillen, A. J.; Murzin, D. Y.; Koningsberger, D. C.; De Jong, K. P. *J. Catal.* **2004**, *226*, 215−225.
(29) Serp, P.; Corrias, M.; Kalck, P. *Appl. Catal., A* **2003**, *253*, 337−358.
(30) Van Dillen, A. J.; Geus, J. W.; Hermans, L. A. M.; Van der Meijden, J. *Stud. Surf. Sci. Catal.* **1977**, *2*, 677.
(31) De Jong, K. P.; *Stud. Surf. Sci. Catal.* **1991**, *63*, 19−36.
(32) Burattin, P.; Che, M.; Louis, C. *J. Phys. Chem. B* **1997**, *101*, 7060−7074.
(33) Burattin, P.; Che, M.; Louis, C. *J. Phys. Chem. B* **1998**, *102*, 2722−2732.
(34) Burattin, P.; Che, M.; Louis, C. *J. Phys. Chem. B* **1999**, *103*, 6171−6178.
(35) Nares, R.; Ramirez, J.; Gutierrez-Alejandre, A.; Louis, C.; Klimova, T. *J. Phys. Chem. B* **2002**, *106*, 13287−13293.
(36) Wigmans, T.; van Doom, J.; Moulijn, J. A. *Surf. Sci.* **1983**, *135*, 532.
(37) Prinsloo, F. F.; Hauman, D.; Slabbert, R. *Carbon'01, An International Conference on Carbon*; Lexington, KY, United States, 2001; pp 940−947
(38) Bitter, J. H.; Van der Lee, M. K.; Slotboom, A. G. T.; Van Dillen, A. J.; De Jong, K. P. *Catal. Lett.* **2003**, *89*, 139−142.
(39) Toebes, M. L.; Bitter, J. H.; Van Dillen A. J.; De Jong, K. P. *Catal. Today* **2002**, *76*, 33.
(40) Toebes, M. L.; van Heeswijk, J. M. P.; Bitter, J. H.; Van Dillen, A. J.; De Jong, K. P. *Carbon* **2004**, *42*, 307−315.

rate 5 K/min) for 1 h. After cooling to room temperature and subsequent gradual exposure to air, the catalyst was collected.

20 wt % Ni on silica (Degussa, Aerosil, specific surface area 200 m^2/g) was prepared via the same procedure as described for CNF.

Nickel Ion Concentration during Deposition Precipitation and Loading. The aqueous nickel-ion concentrations during the DP process were determined via flame atomic absorption spectroscopy (AAS) at 352.5 nm using a Varian Spectra 10 apparatus. Samples (1 mL) were collected from the DP solution, acidified with diluted HNO_3, and diluted to a concentration between 1 and 25 ppm, which was the range of the nickel calibration curve.

Nickel ion adsorption on the support, before urea was added to the suspension, was determined both via the liquid phase as described above and via the "solid phase". In the latter case, 300 mg of support were suspended in 250 mL of water, and the pH was set to ~3.5. Next 371 mg of nickel nitrate were added to the solution. The reaction mixture was headed to 363 K. After 0.5 h the support was collected by filtration, washed thoroughly, and dried at 393 K. 100 mg of CNF-O (including the adsorbed nickel) were resuspended in 50 mL of 0.1 mol/l HNO_3; after filtration the nickel ion concentration in the aqueous phase was determined via AAS as described above. For silica 150 mg were resuspended in 50 mL of 0.1 mol/L HNO_3 to analyze the amount of nickel adsorbed.

With thermal gravimetric analysis (TGA) the loading of nickel on the CNF was verified. The loaded fibers were heated in 5 vol % oxygen in nitrogen to 1173 K (ramp 5 K/min). Resulting yields were corrected for the amount of nickel in unloaded CNF-O fibers.

Characterization. Samples were prepared for TEM by suspending the fibers in ethanol under ultrasonic vibration. Some drops of the thus produced suspension were brought onto a holey carbon film on a copper grid. The grids were transferred to a Technai transmission electron microscope operated at 200 keV with an FEG. Scanning Electron Microscopy, performed with a Philips XL30 FEG apparatus, was used to assess the morphology of the carbon nanofiber bodies.

For XRD an Enraf Nonius PDS 120 powder diffractometer system equipped with a position-sensitive detector with a 2 theta range of 120° using Co $K\alpha_1$ ($\lambda = 1.788\,97$ Å) radiation was used.

Prior to the physisorption measurement the samples were dried at 473 K. For N_2 physisorption at 77 K a Micromeritics Tristar 3000 apparatus was used.

The total pore volume based on mercury porosimetry was determined using Pascal 440 apparatus at 296 K. With this setup pore radii between 7500 and 1.8 nm were analyzed.

Results and Discussion

Carbon Nanofiber Supports. The as-synthesized (CNF-A), the purified and surface-oxidized (CNF-O) and the oxidized-reduced (CNF-OR) carbon nanofibers have been characterized by XRD (Figure 1). A broad and intense diffraction line close to 30° 2θ and weaker lines at 50°, 62° and 95° reveal the graphite-like character of the CNF materials. With the CNF-A the presence of metallic nickel is apparent from the XRD pattern. For CNF-O and CNF-OR this nickel has been largely removed although some encapsulated nickel is still present (<0.1 wt %).

SEM and TEM images of CNF-A are displayed in Figure 2. The macroscopic CNF bodies or skeins have a size of 0.3−0.8 mm. The mechanically strong bodies consist of interwoven fibers with a diameter of 20−50 nm (Figure 2B). The individual fibers consist of turbostratic graphite-like material, while the graphene sheets run under an angle with the main axis of the fiber (Figure 2C). The so-called fishbone- or herringbone-type arrangement of the graphene sheets is characteristic of the carbon nanofibers. It has been checked that neither the mesoscopic (Figure 2B) nor the microscopic (Figure 2C) structure did

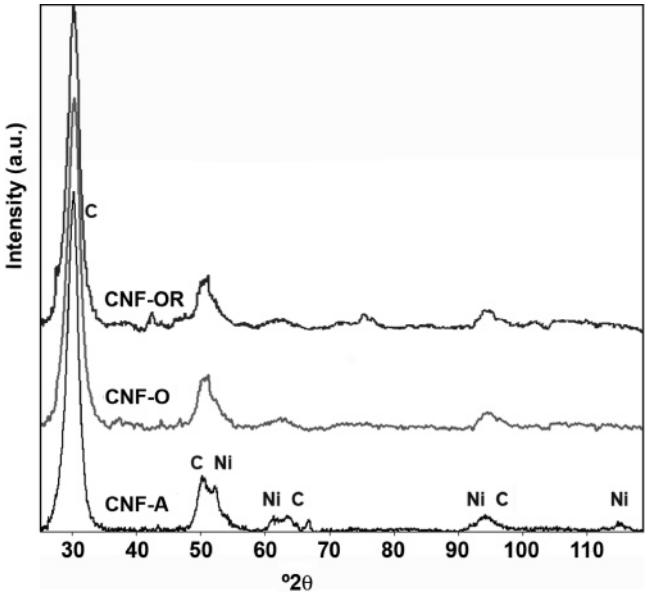

Figure 1. X-ray diffraction pattern of untreated (CNF-A), surface oxidized (CNF-O), and reduced carbon nanofibers (CNF-OR).

change upon further treatment of the fibers (samples CNF-O, CNF-OT, CNF-OR).

The texture of the support materials has been studied using nitrogen physisorption and mercury porosimetry, the results of which are summarized in Table 1. From t-plot analysis it was established that micropores (<2 nm) were absent in all the materials studied. The specific surface area of the CNF-O and CNF-OR materials were ~150 m^2/g. The pore volume obtained from nitrogen physisorption of 0.3−0.4 mL/g (Table 1) must be present in pores <100 nm in view of the technique limitations. These mesopores represent the open space between closely packed fibers. The presence of macropores can be deduced from the larger pore volume obtained from Hg-porosimetry compared to that obtained from N_2 physisorption. For CNF-O the macropore volume amounts to 0.26 mL/g and is in line with the large voids between fibers that can be observed in Figure 2B.

In view of the absence of micropores in the CNF skeins the equilibration during titration was fast in all cases. For CNF-O the amount of base added to arrive at a certain pH in all cases exceeds the amount needed with the blank solution (Figure 3). From this the acidic surface groups present on CNF-O are revealed. The oxidation treatment applied to obtain CNF-O is known to lead to formation of a range of oxygen-containing groups, viz. carboxylic acid, carboxylic anhydride, lactone, phenolic quinone, and cyclic peroxide groups.[17,19,25,41,42] Roughly speaking, carboxylic acid groups display pK_a < 5 and OH groups attached to large polyaromatic rings pK_a = 8−9.[43−47] The broad range of pK_a values is reflected by the low slope of the titration curve for CNF-O compared to that of the blank. The differences between the blank and CNF-O curves has been

(41) Ros, T. G.; Van Dillen, A. J.; Geus, J. W.; Koningsberger, D. C. *Chem.—Eur. J.* **2002**, *8*, 1151−1162.
(42) Hoogenraad, M. S. Ph.D. Thesis, Utrecht University, 1995.
(43) McCann, G. M.; McDonnell, C. M.; Magris, L.; O'Ferrall, R. A. M. *J. Chem. Soc., Perkin Trans. 2* **2002**, *4*, 784−795.
(44) Pines, E.; Magnes, B.-Z.; Lang, M. J.; Fleming, G. R. *Chem. Phys. Lett.* **1997**, *281*, 413−420.
(45) Abd El Wahed, M. G. *Acta Chim. Hung.* **1990**, *127*, 51−56.
(46) Weller, Z. *Elektrochem. Angew. Phys. Chem* **1952**, *56*, 662−664.
(47) Kieffer, R. *C. R. Hebd. Seances Acad. Sci.* **1954**, *238*, 700.

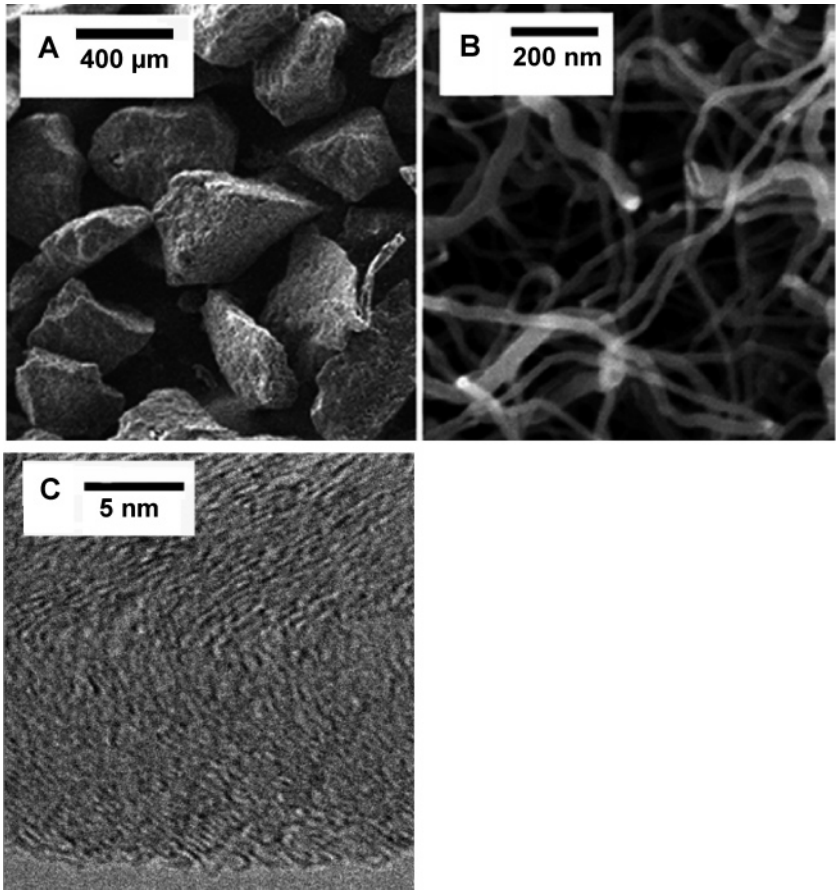

Figure 2. (A) Carbon nanofiber bodies at low magnification in SEM; (B) at higher magnification the interwoven fibers are visible in the SEM image; (C) HRTEM image of a single fishbone-type carbon nanofiber.

Table 1. Physical Properties of Different Treated Carbon Nanofiber Support Materials[a]

CNF-type	S_{BET} [m^2/g]	PV_{meso} [mL/g]	ϕ_{pore} [nm]	PV_{total} [mL/g]
CNF-O	150	0.32	15	0.58
CNF-OR	152	0.36	14	n.d.
CNF-OT	172	0.37	14	n.d.

[a] n.d. = not determined. PV_{meso} = mesopore volume. ϕ_{pore} = average pore diameter. PV_{total} = total pore volume based on Hg porosimetry.

Table 2. Oxygen Containing Surface Groups on Different Treated Carbon Nanofibers

	surface groups [mmol/g]			
CNF-type	$pK_a < 5$	pK_a 5–8	pK_a 8–9	total
CNF-O	0.17	0.15	0.08	0.40
CNF-OR	0.03	0.15	0.13	0.31
	surface groups [mmol/g]			
CNF-type	pK_b 4–5	pK_b 5–8	pK_b 8–9	total
CNF-OT	0.03	0.03	0.00	0.06

established at different pH values, and from that the amounts of acid groups with different ranges of pK_a have been calculated and are summarized in Table 2. Taking into account the specific surface area (Table 1) and the total number of sites with a $pK_a < 8$ of 0.32 mmol/g (Table 2) we calculate 1.3 oxygen-containing surface groups per nm^2 for CNF-O. This number is well in line with a study of Toebes et al.[40] on the surface oxidation of carbon nanofibers.

For CNF-OR the results of Figure 3 and Table 2 show that the total number of oxygen-containing groups has not decreased to a large extent as a result of the reduction treatment. However, the number of strongly acidic sites in particular carboxylic acid groups ($pK_a < 5$) has decreased substantially. From the data of Table 2 it is apparent that the number of phenol-type groups ($pK_a = 8-9$) on CNF-OR is larger than that of CNF-O. The chemical reduction of carboxylic acid groups with $LiAlH_4$ has clearly led to formation of additional phenol-type groups although the total number of groups has decreased slightly.

With CNF-OT the pH curve runs left of the blank curve indicating the base character of this material. In line with literature,[18,48] thermal treatment has led to removal in particular of carboxylic acid groups that give rise to formation of basic groups on one hand and reduction of the total number of oxygen-containing groups on the other hand. Ether-like, carbonyl-type, or pyrone-type groups have been proposed as basic sites on carbon surfaces.[49] The total number of basic sites with $pK_b < 8$ is obtained by the differences at pH = 6 assuming equal alkali consumption at pH = 10 and amounts to 0.06 mmol/g (cf. Table 2).

Deposition Precipitation Experiments. Deposition precipitation of nickel onto a suspended silica support was monitored with pH measurements. The results are summarized in Figure 4 (curve 4) together with blank experiments of urea only (curve 1), urea with silica (curve 2), and urea with nickel nitrate (curve

(48) Boehm, H. P. *Adv. Catal.* **1966**, *16*, 179.
(49) Voll, M.; Boehm, H. P. *Carbon* **1971**, *9*,481.

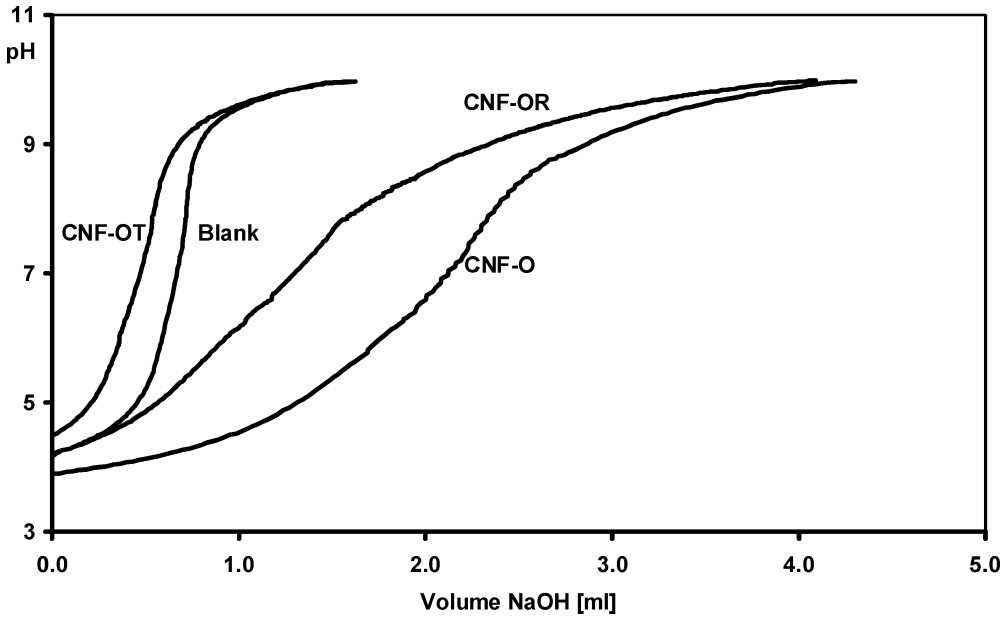

Figure 3. Titration curves of CNF-O, CNF-OR, CNF-OT, and the blank solution without support.

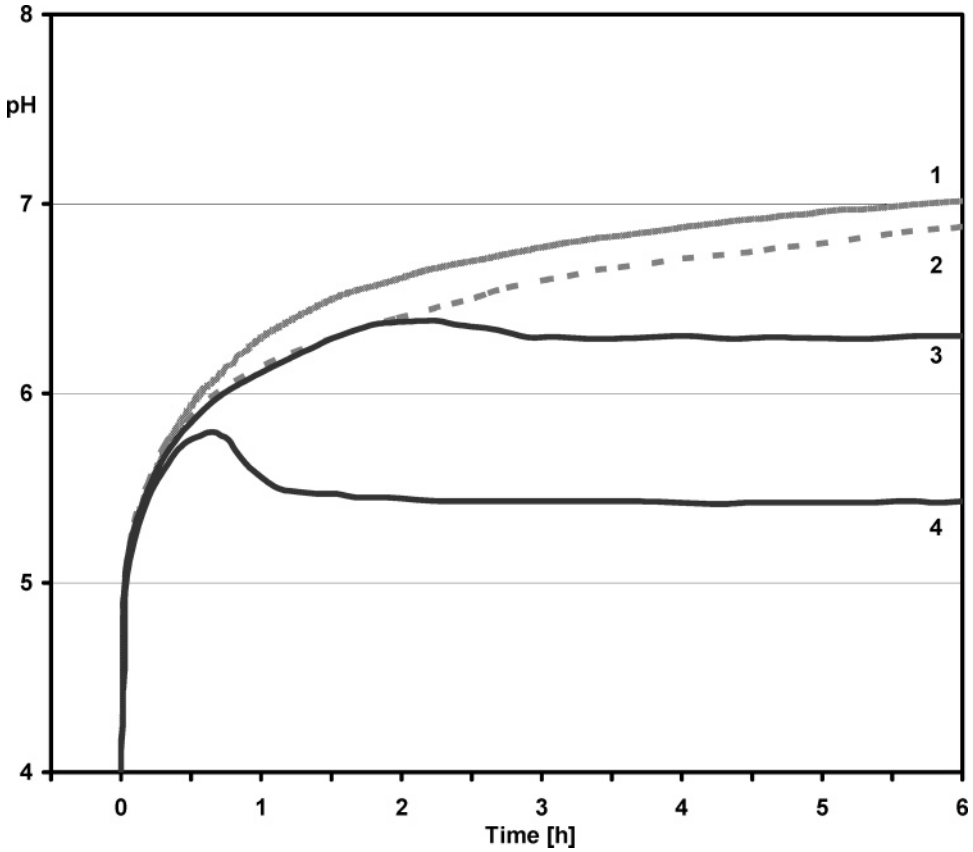

Figure 4. pH development during DP process for nickel-on-silica at 363 K with 15.3 mmol/L urea. (1) Urea only; (2) 1.2 g/L silica; (3) 5.1 mmol/L nickel nitrate; (4) 5.1 mmol/L nickel nitrate and 1.2 g/L silica.

3). In all cases an initially rapid increase of pH is observed. This increase is caused by neutralization of the nitric acid present by the ammonium hydroxide generated by the hydrolysis of urea, reaction 1.

$$CO(NH_2)_2 + 3\,H_2O \rightarrow CO_2\,(g) + 2\,NH_4^+ + 2\,OH^- \quad (1)$$

At more elevated pH the rate of increase drops for a number of different reasons. For the urea-only system the pH levels at around 7 due to, on one hand, buffering effects and conversion of carbon dioxide into bicarbonate and, on the other hand, evaporation of ammonia, reaction 2.

$$NH_4^+ + OH^- \rightarrow NH_3\,(g) + H_2O \quad (2)$$

With both urea and silica present the pH runs slightly below the urea-only case (Figure 4, curve 2). Earlier Burattin et al.[33] have explained this deviation between the two curves as being

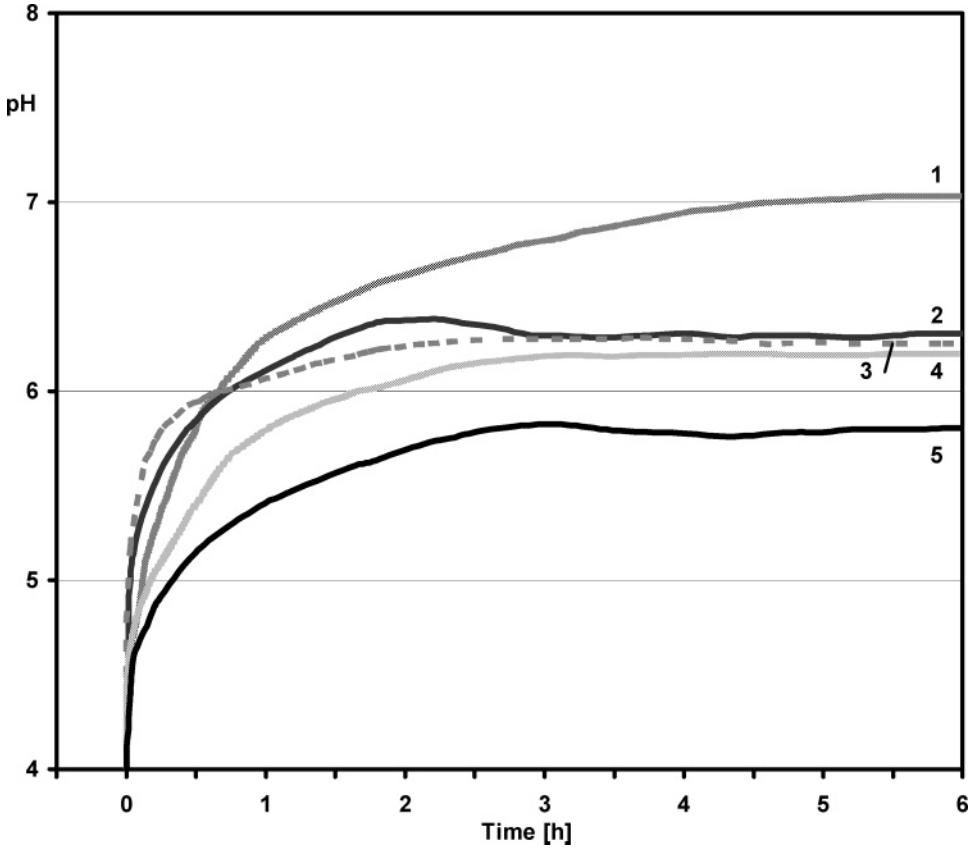

Figure 5. pH development during DP process for nickel-on-CNF at 363 K with 15.3 mmol/L urea. (1) 1.2 g/L CNF-O; (2) 5.1 mmol/L nickel nitrate; (3) 5.1 mmol/L nickel nitrate and 1.2 g/L CNF-OT; (4) 5.1 mmol/L nickel nitrate and 1.2 g/L CNF-OR; (5) 5.1 mmol/L nickel nitrate and 1.2 g/L CNF-O.

due to the acid-reacting silanol groups present at the support. Since the number of OH groups on silica ($\sim$ 2.2 mmol/g[48]) is much larger than that on CNF-O it is apparent that the acidity and related nickel ion adsorption of silanol groups are limited, as compared to that of carboxylic acid groups, and has only little impact on the pH curve. With urea and nickel nitrate (Figure 4, curve 3) the pH curve coincides with urea only until pH = 5.5. Beyond pH = 5.5 the presence of nickel ions appears to retard the rise of pH. Hydrolysis of nickel ions starts at this value of pH according to reaction 3

$$[Ni(OH_2)_6]^{2+} + OH^- \rightarrow [Ni(OH)(OH_2)_5]^+ + H_2O \quad (3)$$

and in line with earlier proposals.[9,30,33] The maximum of the pH curve (curve 3, pH = 6.4, t = 2.0 h) is attributed to a supersaturated solution and the nucleation of a solid phase, viz. $Ni(OH)_2$.[9] Subsequently, the pH drops slightly to a (pseudo-)-steady state value of 6.3. This value coincides roughly with the solubility product of nickel hydroxide.[50−51]

With urea, nickel, and silica present (Figure 4, curve 4) a maximum of pH occurs at t = 0.7 h and pH = 5.8. Clearly, nucleation of a new phase occurs much earlier in the process of urea hydrolysis pointing to formation of a nickel phase that is more stable than bulk $Ni(OH)_2$. According to the literature[33,34] this phase is turbostratic nickel hydroxide in strong interaction with silica that is converted into a nickel phyllosilicate after prolonged precipitation. For this nickel phase the solubility as apparent from the steady state pH = 5.4 is lower than that of unsupported nickel hydroxide (pH = 6.3). The nucleation has been suggested to be preceded by nickel ion adsorption, a theme that we will discuss more extensively below. Here it suffices to say that the pH curves 3 and 4 hardly deviate from each other prior to the maximum in curve 4, which might suggest that nickel ion adsorption onto silica is not extensive below pH = 5.8.

As a preliminary conclusion we propose that the adsorption of nickel ions and the nucleation coincide and can be represented by reaction 4.

$$Si{-}OH + [Ni(OH)(OH_2)_5]^+ + OH^- \rightarrow Si{-}O{-}Ni(OH)(OH_2)_4 + 2\,H_2O \quad (4)$$

The pH curves of deposition precipitation onto CNF supports together with relevant blank experiments are summarized in Figure 5. From the experiment with urea and CNF-O (curve 1) it appears that the pH levels off slightly above pH = 7. In fact this curve coincides largely with curve 1 of Figure 4 (urea only) thus proving that the number of acid groups of CNF-O is not sufficient to affect significantly the pH curve. From the acid site density (Table 2) and the amount of CNF-O in the reaction vessel, the total amount of support acid groups with $pK_a < 5$ can be calculated to be 0.2 mmol/L whereas the initial urea concentration is 15.3 mmol/L. These values rationalize the very limited impact of CNF-O on the pH increase.

The precipitation of unsupported nickel (no support, curve 2 in Figure 5) has been discussed above. For the Ni/CNF-OT (curve 3) the pH increase largely coincides with curve 2. The

(50) Plyasunova, N. V.; Zhang, Y. Muhammed, M. *Hydrometallurgy* **1998**, *48*, 43.
(51) Richens, D. T. *The chemistry of aqua ions*; Wiley-VCH: New York, 1997.

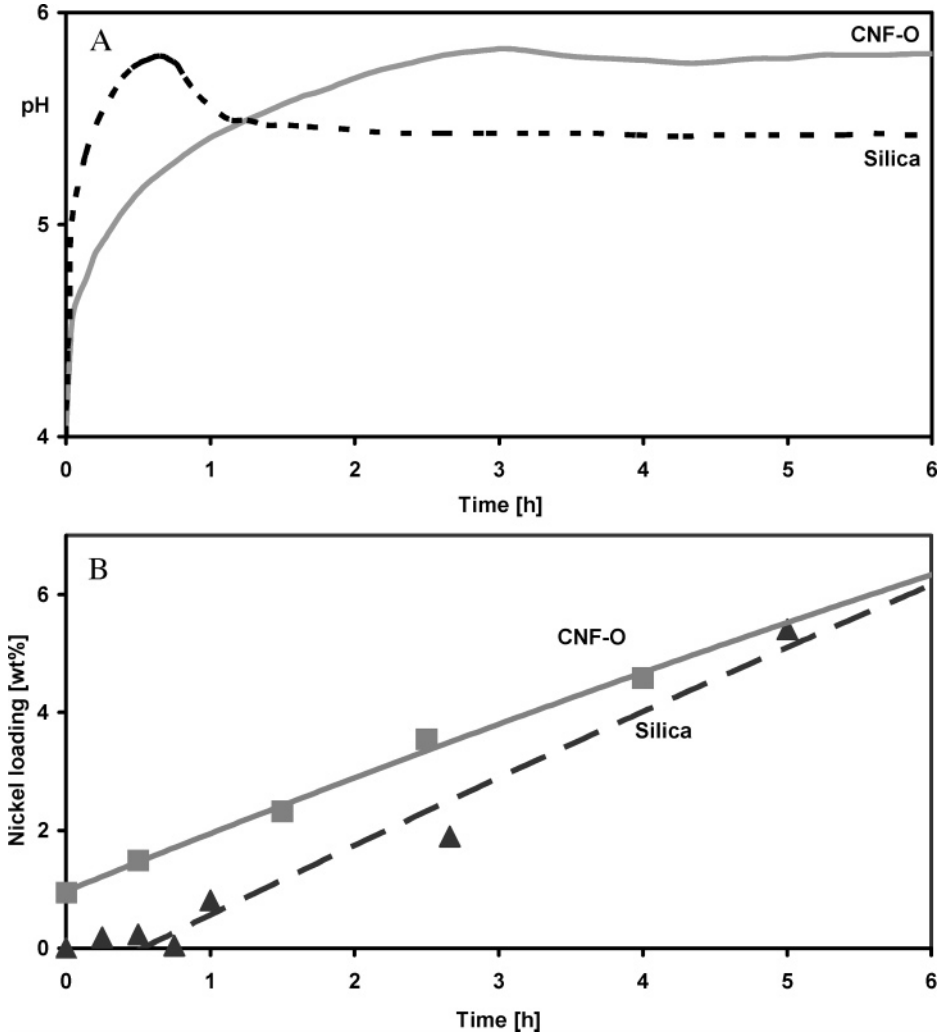

Figure 6. (A) pH curves of DP process onto CNF-O and silica, (B) nickel loading as function of deposition time.

initial pH rise is slightly steeper, and it is tempting to ascribe this to basic groups present on this support (Table 2). Admittedly, also the number of basic groups is small, and a full explanation for the steeper rise is lacking at this point in time. More importantly, the precipitation of nickel with CNF-OT largely takes place at pH = 6.3, very close to the precipitation plateau for bulk nickel hydroxide. From this we expect that nickel hydroxide precipitates largely separate from the support with CNF-OT. Further characterization of the samples obtained will shed further light on this (vide infra). For CNF-OR similar results are obtained (Figure 5, curve 4) albeit that at intermediate time (t < 3 h) a more significant deviation from the blank experiments is apparent. This deviation is now first discussed for CNF-O (Figure 5, curve 5).

With CNF-O (Figure 5, curve 5) the pH increase drops below that of the blanks (curves 1 and 2) already at pH = 4.5, close to time zero. Nucleation of a new phase, most likely nickel hydroxide, is characterized by a maximum of pH = 5.8 that occurs much later, viz. t = 2.8 h. Again, the number of acid groups on CNF-O is by far not sufficient to delay the rise of pH over prolonged times. The only explanation that remains is that significant amounts of nickel-containing species are deposited prior to maximum pH being reached. Since the pH values apparent with CNF-O are significantly below that observed with CNF-OT and CNF-OR, it is likely that a nickel phase interacting with CNF-O is obtained.

To obtain more insight we have determined the amounts of nickel present on the silica and the CNF-O supports as a function of time. The results are summarized in Figure 6. With silica until t = 0.7 h the loading of nickel is zero within the experimental error. Beyond t = 0.7 h the loading seems to increase linearly with time although data do not allow firm statements about the kinetics of deposition. After 24 h (data not shown) with SiO_2, quantitative precipitation of Ni^{2+} has taken place at a final pH = 5.4, whereas about 80% of Ni^{2+} has been removed from solution with CNF-O at a final pH = 5.8.

With silica, extensive nickel ion adsorption does not take place for pH < 5.8 and adsorption coincides with nucleation of a new nickel phase (reaction 4) at the maximum of the pH curve. The nickel loading at zero time, i.e., before addition of urea, for CNF-O amounts to 0.85 wt % Ni, which corresponds to 0.14 mmol of nickel per g of support. Since hydrolysis of the nickel aqua ions does not take place at such a low pH, the adsorption is described by reaction 5.

$$\mathrm{CNF{-}COOH + Ni(OH_2)_6^{2+} + OH^- \rightarrow CNF{-}COO{-}Ni(OH_2)_5^{+} + 2\,H_2O} \quad (5)$$

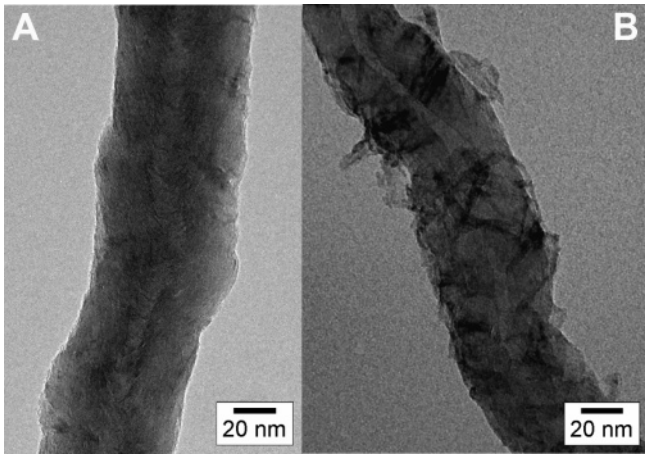

Figure 7. TEM image of a bare CNF (A) and a dried nickel hydroxide loaded CNF-O fiber (B).

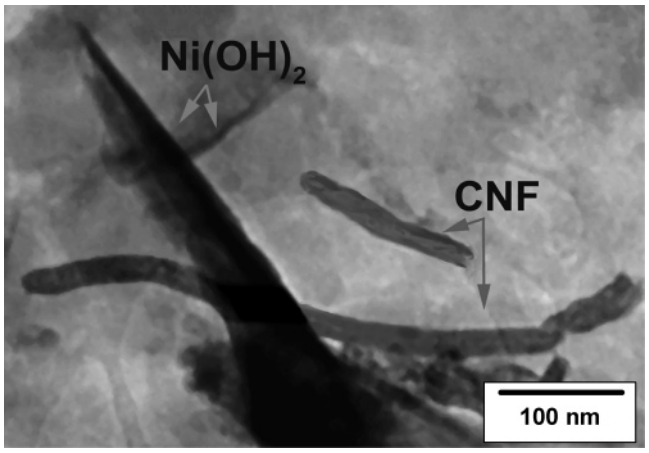

Figure 8. TEM image of large platelets of nickel hydroxide (dark) which are separated from CNF-OR fibers.

If we assume that acid sites with a $pK_a < 5$ are involved in reaction 5, the ratio of nickel over acid sites amounts to 0.84 mol/mol, close to unity. Beyond time zero a smooth and linear increase of the nickel loading with time is observed for CNF-O (Figure 6B). At the maximum pH = 5.8 at $t = 2.8$ h the nickel loading from interpolation of the data is estimated at 3.8 wt % Ni or 0.65 mmol/g that corresponds to a Ni/acid-site ratio of 3.8 ($pK_a < 5$) or 2.0 ($pK_a < 8$) mol/mol. The growth of binuclear or larger complexes of nickel on the CNF-O support coincides with extensive consumption of hydroxyl ions as revealed by a significant delay of the increase of pH between pH = 3.5 to pH = 5.8 (Figure 6A). This consumption of hydroxyl ions can be accounted for by reaction 6 for which binuclear nickel complexes are assumed.

$$\mathrm{CNF{-}COO{-}Ni(OH_2)_5^{+} + Ni(OH_2)_6^{2+} + 3\,OH^{-} \rightarrow CNF{-}COO{-}Ni{-}OH{-}Ni(OH)_2 + 11\,H_2O} \quad (6)$$

A similar but less extensive adsorption and hydrolysis of nickel ions onto CNF-OR brought about by remaining carboxylic acid groups (0.3 mmol/g) is proposed to have caused the somewhat retarded pH increase apparent in Figure 5, curve 4.

Beyond $t = 2.7$ h it is assumed that the small nickel clusters assist in nucleation that leads to a nickel hydroxide phase (pH = 5.7). To study this phase we turn in the next section to the characterization of the CNF-supported nickel samples obtained after washing and drying.

Comparison of the pseudo steady region of nickel deposition (Figure 6, $t = 1-5$ h) shows that the rate of deposition onto silica exceeds that onto CNF-O. It has been argued in the past[9] that the rate-determining step for DP is the hydrolysis of urea, the rate of which is not dependent on pH. However, the evaporation of ammonia (reaction 2) will be more important at more elevated pH thus lowering the selectivity of the utilization of urea for precipitation of nickel hydroxide. The lower steady-state pH with silica, therefore, gives rise to a higher rate of nickel deposition.

Characterization of Nickel-Loaded Carbon Nanofibers. The TEM images of CNF-O and Ni/CNF-O obtained by deposition precipitation are displayed in Figure 7. The rather smooth unloaded carbon nanofiber (Figure 7A) has turned into a fiber with many striations (Figure 7B). We assign the striations to platelets of nickel hydroxide with dimensions of 40−50 nm along the basal plane and 5−10 nm thicknesses. The platelets adhere to the surface of CNF-O as can be deduced from Figure

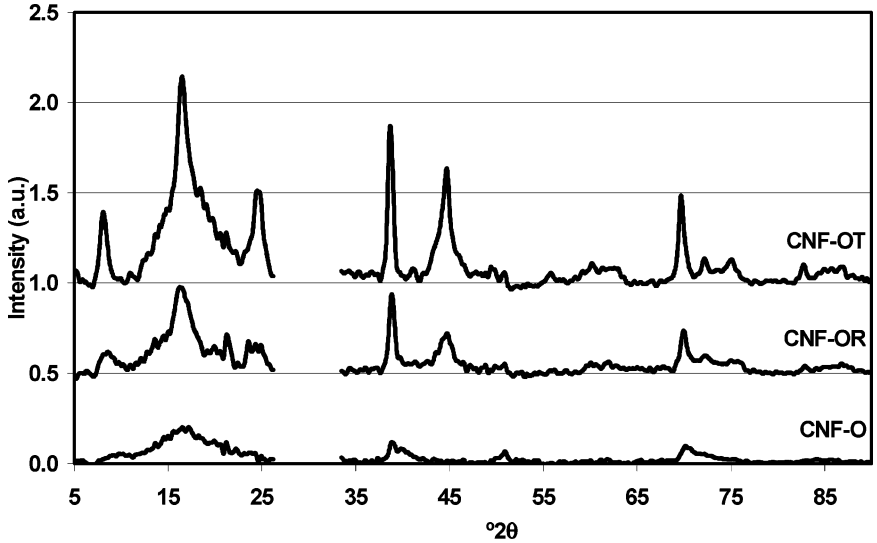

Figure 9. XRD patterns of dried nickel hydroxide precipitates on CNF-O, CNF-OR, and CNF-OT. Patterns were normalized to the graphite (002) reflection, and the graphite contributions have been subtracted.

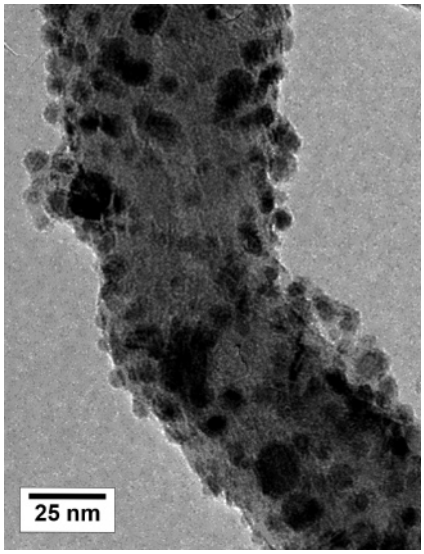

Figure 10. TEM image of nickel particles dispersed on CNF-O after reduction at 773 K.

7B and from the fact that more extensive TEM studies revealed the absence of free nickel hydroxide platelets on the carbon film. Some platelets stick out of the fiber and are most likely edge bonded, whereas other platelets run parallel with the main axis of the fiber and adhere via the basal plane of the nickel hydroxide. For Ni/CNF-OR and Ni/CNF-OT, electron microscopy images were obtained as well and a representative one for both samples is shown in Figure 8. With the lower magnification of Figure 8, carbon nanofibers (~30 nm diameter) and a large platelet of nickel hydroxide (>500 nm) separate from each other are apparent. This points to precipitation of nickel hydroxide in the bulk solution as was already suggested before upon considering the pH curves of Figure 5.

XRD patterns of the dried samples corrected for graphite contributions are shown in Figure 9. Broad diffraction lines for the nickel hydroxide phases are apparent in all cases. The intensities of peaks do vary considerably, however, for the samples with similar nickel loadings. The low-angle diffraction line peaks around 17° 2θ which corresponds to a d-value of 6.2 Å characteristic of the stacking in a layered basic nickel carbonate, e.g., $Ni(OH)_2CO_3 \cdot 4H_2O$.[52] The shoulder of the main peak at ~14° 2θ corresponds to a d-value of 7.25 Å, most likely connected to the presence of α-$Ni(OH)_2$ platelets.[32] The low-angle diffraction line at ~7° 2θ (d =~12 Å) we could not attribute to a known phase. For the CNF-OR and the CNF-OT supported samples, more intense diffraction patterns are obtained with an additional peak at 23° 2θ or d = 4.6 Å assigned to the (001) line of β-$Ni(OH)_2$,[32] a more ordered form of nickel hydroxide. Clearly, larger and more ordered platelets of nickel hydroxide are present in the latter two samples, again in accordance with TEM results. A closer inspection of the 17° 2θ lines of CNF-OT and CNF-OR sample suggests a bimodal distribution of platelets. In other words next to large crystals of nickel hydroxide separate from the support, some smaller platelets might be present.

Briefly, we return to the pH data of Figure 5 that reveal a lower steady-state pH (t > 3 h) for precipitation onto CNF-O (curve 5) than for unsupported nickel hydroxide (curve 2). Following the above characterization the lower pH for CNF-O cannot be due to a different nickel phase (cf. Figure 9). Tentatively, the lower pH is ascribed to kinetic phenomena, viz. the much higher surface area of the nickel hydroxide phase for the supported case leads to faster precipitation that maintains a lower pH. This kinetic basis of the selective deposition on Ni-$(OH)_2$ onto CNF-O is less "robust" than the thermodynamic basis with silica that relies on a more stable nickel hydroxide phase. This conclusion is supported by the experimental observation that a powdered CNF support is mandatory to prevent bulk precipitation during the preparation process, whereas DP with silica can also be carried out with granules.[31]

For sample Ni/CNF-O after reduction at 773 K, TEM results are displayed in Figure 10. The metallic nickel particles are evenly distributed over the fibers and well dispersed with an average particle size of 8 nm. The latter average particle size has been confirmed by XRD line broadening (data not shown).

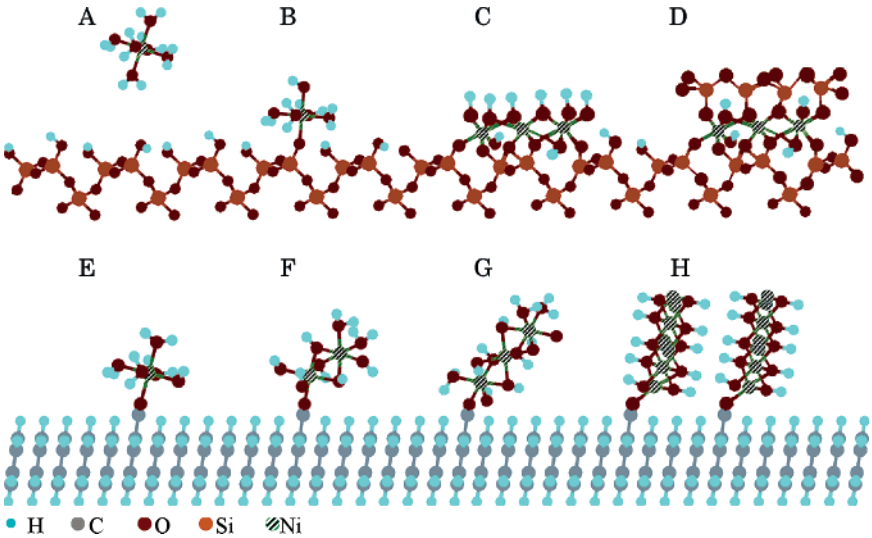

Figure 11. Schematic representation of the mechanism of deposition precipitation of nickel. Top: Nickel deposition precipitation on silica; (A) before nucleation there is no significant interaction between silanol groups and $Ni(OH_2)_6^{2+}$; (B) nucleation on silica support at pH = 5.8; silanol groups interact with nickel ions, which results in the formation of $Si-O-Ni(OH)(OH_2)_4$. (C) Nickel hydroxide is formed at pH of 5.4 and (D) the final nickel phylosillicates. Bottom: Precipitation on CNF-O (Figure 11E−H). (E) Nickel ion adsorption takes place on carboxyl groups; (G) nucleation of $Ni(OH)_2$ at pH = 5.8; (H) growth of $Ni(OH)_2$ sheets at pH = 5.7.

The thermal stability of this Ni/CNF-O catalyst is high, as is apparent from the particle size in combination with the reduction temperature. A more detailed study of the final metallic catalyst including stability and catalytic properties is outside the scope of this paper and will be published elsewhere.

Mechanism of Deposition Precipitation of Nickel. In Figure 11 the proposed model for precipitation of nickel onto silica and carbon is summarized. The mechanism for nickel-on-silica (A−D) resembles that described by Buratin et al.[33] with one exception; viz. ion adsorption does not take place prior to the nucleation of the supported nickel phase at our experimental conditions (Figure 11A). At nucleation silanol groups interact with nickel ions which results in the formation of Si−O−Ni-$(OH)(OH_2)_4$ (Figure 11B and C). The strong chemical interaction between nickel hydroxide and silica is indicated by the formation of nickel phyllosilicate (Figure 11D).

For the carbon support with carboxylic acid groups, nickel ion adsorption does occur prior to nucleation of $Ni(OH)_2$, Figure 11E. Starting at pH = 3.5, all acid sites are already occupied by nickel ions, while close to nucleation (pH = 5.8) about 4 nickel ions per acid site have been adsorbed (Figure 11F and G). Some of these small nickel clusters serve as nucleation sites for the formation of nickel hydroxide platelets (Figure 11H). Growth of these platelets occurs at pH = 5.7, just below the pH at nucleation.

Conclusions

Deposition precipitation of nickel hydroxide onto silica and modified carbon nanofiber support material has been studied by time dependent pH and metal loading studies in combination with characterization of the dried catalyst precursors. With silica the previously studied strong interaction between the deposited nickel hydroxide or nickel phyllosilicate and the support is apparent from the low steady-state pH (pH = 5.4) at which precipitation takes place. From a study of the extent of nickel deposition onto the silica with time of precipitation, it is clearly shown that prior to nucleation of the nickel phase on the support (pH = 5.8) no nickel ion adsorption occurs. From this it is strongly suggested that nickel ion adsorption coincides with the nucleation phase for the silica support. For surface-oxidized carbon nanofibers (CNF-O), extensive adsorption occurs right from the start of the deposition precipitation (pH = 3.5). At the maximum of the pH curve (pH = 5.8) that reveals nucleation of a new phase, already 22% of the nickel present has been deposited onto CNF-O in strong contrast with silica. The steady-state pH at which precipitation takes place (pH = 5.7) is well above that observed with silica and below that of blank experiments thus pointing to deposition of the nickel hydroxide phase onto the carbon support. Characterization of the dried catalysts shows small platelets (40 × 5 nm) of nickel hydroxide adhered to the CNF-O. After reduction of the sample at 773 K a 20 wt % Ni/CNF-O sample is obtained with well-dispersed metallic nickel particles of 8 nm on the carbon nanofibers. The oxidized carbon nanofibers contain acidic groups of the carboxylic-type. After removal of these groups by either chemical reduction or thermal treatment, deposition precipitation takes place separate from the support and large nickel hydroxide platelets (> 500 nm) are observed. Acid groups on the modified carbon support are concluded to play a key role in the success of deposition precipitation of nickel hydroxide onto carbon nanofibers.

Acknowledgment. The authors acknowledge C. van der Spek and J. W. Geus for performing the TEM and SEM measurements and the financial support of STW (Grant UPC 5487).

JA053038Q

(52) Nickel, E. H., Robinson, B. W., Mumme, W. G. *Am. Mineral.* **1993**, *78*, 819.